Journal of Archaeological Science 40 (2013) 2136–2151

Contents lists available at SciVerse ScienceDirect

Journal of Archaeological Science

journal homepage: http://www.elsevier.com/locate/jas

Airborne laser bathymetry – detecting and recording submerged archaeological sites from the air

Michael Doneus [a,b,*], Nives Doneus [b], Christian Briese [b,c], Michael Pregesbauer [b,d], Gottfried Mandlburger [c], Geert Verhoeven [a,b]

[a] Vienna Institute for Archaeological Science, University of Vienna, Franz-Kleingasse 1, 1190 Wien, Austria
[b] LBI for Archaeological Prospection & Virtual Archaeology, Hohe Warte 38, 1190 Wien, Austria
[c] Department of Geodesy and Geoinformation, Vienna University of Technology, Gusshausstrasse 27-29/E120.7, 1040 Wien, Austria
[d] Airborne Technologies GmbH, Viktor Lang Strasse 8, 2700 Wr. Neustadt, Austria

ARTICLE INFO

Article history:
Received 6 November 2012
Received in revised form
17 December 2012
Accepted 19 December 2012

Keywords:
Airborne laser scanning
Airborne laser bathymetry
Archaeological prospection
Underwater
Submerged site
Roman villa

ABSTRACT

A new generation of airborne bathymetric laser scanners utilises short green laser pulses for high resolution hydrographic surveying in very shallow waters. The paper investigates its use for the documentation of submerged archaeological structures, introducing the concept of airborne laser bathymetry and focussing on a number of challenges this novel technology still has to face. Using this method, an archaeological pilot study on the northern Adriatic coast of Croatia has revealed sunken structures of a Roman villa. The results demonstrate the potential of this novel technique to map submerged archaeological structures over large areas in high detail in 3D, for the first time providing the possibility for systematic, large-scale archaeological investigation of this environment. The resulting maps will provide unique means for underwater heritage management.

1. Introduction

Due to its enormous abundance (74% of the Earth's surface – Jensen, 2007) and the various states in which water can exist together with the fact that it can be difficult to obtain in situ point measurements, it is not surprising that considerable research has taken place in the field of water remote sensing. Methods have been developed to measure, inventory, quantify, and predict different hydrological variables such as water-surface extent and temperature, water volume, velocity of waves, organic and inorganic water constituents, or water depth (bathymetry).

Detailed knowledge of water depth, or underwater topography respectively, is essential for many research fields, including hydraulics, hydro-morphology, and hydro-biology. In archaeology, it is the basis for understanding of organisation and distribution of archaeological sites along and within water bodies. Here, special attention has to be paid to intertidal and inshore zones where shipwrecks, fish traps, middens, pile dwellings, weirs, wharves, docks, piers and other maritime infrastructure, various forms of dredging, oyster beds, individual larger objects (e.g. stone anchors), and any kind of submerged structure can be found (Blondel, 2009, pp. 220–221; Bowens, 2009, p. 16; Strachan, 1995).

Also, coastlines have changed due to sea-level rise (Lambeck et al., 2004) and many former coastal sites are now submerged in shallow water, which is in our case study a depth of maximally 2 m below the water surface (see below). Mapping the relief within these areas is therefore important in order to be able to reconstruct former coastlines, identify sunken archaeological structures and recognize navigable areas which can help to locate potential former harbour sites.

Intertidal and inshore areas are, therefore, extremely rich in archaeological information content. Surprisingly, until now archaeology has lacked suitable methods to provide detailed maps of the topography of these shallow underwater bodies. To detect, document, visualise and archaeologically interpret inshore topography and its archaeological remains, an applicable technique would have to fit following requirements: (1) it has to cover large areas in a sufficiently short time; (2) in order to identify archaeological structures, the resulting digital terrain model (DTM) or digital depth model (DDM, Collin et al., 2008) should have high detail (sub-metre), and (3) the depth range should be from the water surface to a few metres below.

* Corresponding author. Vienna Institute for Archaeological Science, University of Vienna, Franz-Kleingasse 1, 1190 Wien, Austria. Tel.: +43 1 4277 40486.
E-mail address: Michael.Doneus@univie.ac.at (M. Doneus).

0305-4403/$ – see front matter © 2012 Elsevier Ltd. All rights reserved.
http://dx.doi.org/10.1016/j.jas.2012.12.021

Currently available methods (Firth, 2011) do not meet these requirements: Due to practical constraints (boat access in areas of extremely shallow water) and depending on the pulse length, waterborne echo sounding has its limitations at shallow water depths (de Jong, 2002, p. 322). Terrestrial surveys, i.e. the use of total station and GPS in water depths of up to three metres are extremely time-consuming, small-scale, and do not generate the necessary detail (Bowens, 2009, pp. 91–95). Airborne laser scanning (ALS) systems (Wehr and Lohr, 1999), used to produce accurate and precise terrain models of land surfaces (Doneus and Briese, 2011), do not penetrate the water column (see below). Airborne photogrammetry has been applied (Carbonneau et al., 2006; Marcus and Fonstad, 2008; Westaway et al., 2001) and although it proves to be a relatively low-cost method that can be used for mapping large areas, its success is strongly depending on water transparency and characterised by many other specific weaknesses such as illumination variations and refraction behaviour (see Carbonneau et al., 2006 for a more in-depth discussion). Finally, underwater surfaces could also be measured using existing hydrographic ALS systems, which have been in use for more than a decade (Guenther et al., 2000b). They are, however, designed for maximum water penetration and the moderate pulse repetition rate results in a rather rough ground sampling distance of several metres (e.g. Cunningham et al., 1998; McNair, 2010, 24 ff.). Therefore, they are not suitable for the archaeological purposes mentioned above.

Only the latest generation of airborne laser bathymetry (ALB) scanner systems which are now becoming available utilise very short and narrow green laser pulses. Our objective, therefore, is: Do these novel instruments meet the aforementioned necessary requirements? And, if yes, does their use have the potential to measure underwater surfaces over large areas in high detail, even revealing archaeological structures in shallow water?

Following our research questions, this paper will present the latest generation of airborne bathymetric laser scanning systems. It is hypothesised that these sensors have a number of advantages, especially for very shallow water volumes, which can lead to a better identification of micro-topographic and archaeological structures. After introducing the physical fundamentals, basic techniques and state of art of ALB, the concept of the new system will be explained. Finally, using an area in the Croatian Northern Adriatic as a case study, its archaeological potential will be illustrated and discussed.

2. Airborne laser bathymetry

During the last 10 years, airborne laser scanning (ALS) systems have found wide application in addition to their well-known archaeological applications (Crutchley and Crow, 2010). More specifically, they have had an important impact on the prospection and documentation of sites and landscapes covered by woodland (Doneus et al., 2008). During data acquisition, ALS systems operate in the near or short-wave infrared wavelength (typically using stable laser sources at a 1064 nm or 1550 nm wavelength), which is largely absorbed by water bodies (Curcio and Petty, 1951). Therefore, conventional ALS systems have a limited applicability under wet conditions (i.e. snow and rain, depending on the utilized wavelength) and when water penetration is desired. In these cases, other wavelengths have to be utilised as laser sources. In order to identify adequate wavelengths, it is necessary to have a proper understanding of the fundamental interactions between electromagnetic (EM) radiation and the water column and how this interplay influences the total radiation that penetrates a water body.

2.1. Underwater laser radiation propagation

The airborne laser pulse always interacts with the three components of shallow water bodies: the water surface, the water column and the benthic or bottom. In the following text, a water body is considered as a complex mix of particles and dissolved substances that, when combined with a specific bottom boundary, yields optical properties that can vary over a large continuum of values (Mobley et al., 2004).

2.1.1. Electromagnetic radiation in pure water

Before delving into the water constituents, it is useful to understand how a pure water column without any organic or inorganic components absorbs and scatters incident optical EM radiation (by absorption it is meant that photon energy is lost due to interaction with water molecules, whereas scattering changes the path of the propagating photons). Fig. 1 summarizes the absorption coefficient $a(\lambda)$, the scattering coefficient $b(\lambda)$ and the total attenuation (extinction) coefficient $c(\lambda)$ (i.e. $a + b$) of pure water molecules at wavelengths from 250 nm (Ultraviolet) to 750 nm (Infrared) and expressed in units of inverse metres (m^{-1}). As these properties only relate to the medium of water, they are both called inherent optical properties (IOP) (Mobley, 1994). More specifically, they are determined irrespective of the ambient EM field and depend only on the medium (Dekker et al., 2002). As both the scattering and absorption coefficient are functions of wavelength, they are denoted as spectral properties.

From Fig. 1, it is obvious that absorption mostly takes place from 540 nm onwards, while in the Ultraviolet (UV) region (<400 nm) molecular water absorption dominates below 320 nm. In the Near-Infrared (NIR; 700 nm–1100 nm) and Short Wavelength Infrared (SWIR; 1100 nm–3000 nm), absorption of the incident EM radiation is extremely high, but scattering is almost non-existent. As scattering is largely dependent on the wavelength, it strongly dominates in the UV and blue spectral region (400 nm–500 nm). From 540 nm wavelengths onwards, molecular water scattering becomes insignificant when compared to the amount of absorption.

The combination of these effects explains why pure deep water bodies are perceived as blue by the human visual system. Moreover, it also explains why water is readily discernible in NIR images, as its high absorption coefficient (Curcio and Petty, 1951) renders its very dark to black in NIR images (Smith and Baker, 1981; Engman and Gurney, 1991). From a remote sensing point of view, these NIR and SWIR regions are perfect for discriminating land from pure water, as they yield a very high contrast between the dark water and reflective land features. Looking again at the visible range, the low attenuation in the 420 nm–540 nm spectral region seems most promising to penetrate through the water column and obtain depth (i.e. bathymetric) information.

Besides the absorption and scattering processes, large-scale salinity and temperature variations create changes in refraction of propagating EM radiation, a phenomenon called turbulence. Apart from some influence in very clear water, particle scattering mostly dominates underwater light propagation (Mullen, 2009). The next section describes the effects of these (in)organic constituents in more detail.

2.1.2. Spectral response of water with (in)organic constituents

For the archaeological purposes outlined in the introduction, additional optically active material such as suspended sediments, phytoplankton, and yellow substances have to be taken into account. This yellow substance, also known as coloured/chromophoric dissolved organic matter (CDOM) or “Gelbstoff”, is decayed organic material that has been dissolved in fresh or marine waters (Davies-Colley and Vant, 1987). Together with the other

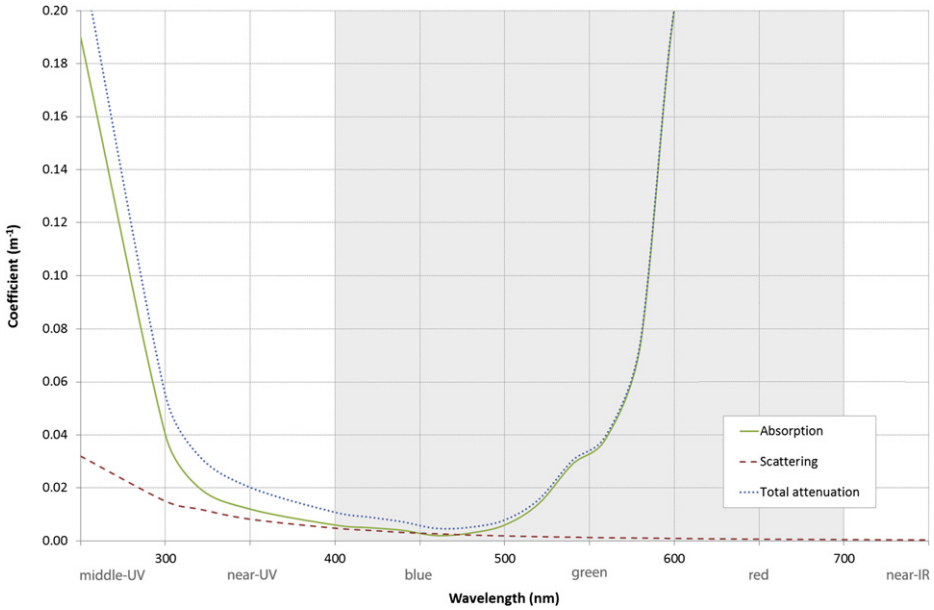

Fig. 1. How EM radiation propagates in clear water is determined by absorption and scattering coefficients. This graph displays the scattering, absorption and total attenuation of EM radiation in pure water from 250 nm UV radiation to 750 nm NIR wavelengths (data from Bukata et al., 1995).

constituents, they affect the absorption and scattering of radiant energy (Han and Rundquist, 2003; Kirk, 1994).

Most substances are large enough to be Mie scatterers (Wojtanowski et al., 2008) and, thus, scatter quite uniformly across the visible spectrum (Piech and Walker, 1971). However, the amount of scattering and spectral absorption of mineral particles is still very different from phytoplankton (Fig. 2). For example, due to its chlorophyll content phytoplankton mainly absorbs in the blue and red visible spectrum (Gitelson, 1992), while inorganic particles often display a high absorption of the Near-Ultraviolet (NUV) and blue spectrum (Mobley et al., 2004). Although CDOM does not really scatter light, it has a significant effect on short-wavelength NUV and blue absorption. An increasing amount of yellow substance will alter the water colour to green, pale-yellow and even brown (Davies-Colley and Vant, 1987; Kirk, 1994). This means that in productive waters such as oceanic upwelling areas or coastal waters with abundant phytoplankton, the EM radiation penetration zone is more or less limited to the green wavelengths (Kirk, 1994). Only in fresh waters red visible radiation might penetrate equally far as green light (or even further). Of course, the specific IOPs of every water column are bound to the particular type and amount of minerals, yellow substance and phytoplankton species.

Even though the water-leaving radiance of an incident laser is governed by this (in)organic matter, the depth and spectral reflectance of the bottom substrate also largely defines the total radiometric signal in shallow waters (Silva et al., 2008; Mobley et al., 2004). Finally, the angular geometry of the incident laser beam is also of importance (Lee et al., 2011), because it can influence the beam deflection.

2.1.3. *The green laser solution*

Taking all the factors into account, it can be stated that the effective usable spectral region for water penetration is shifted to longer wavelengths with respect to pure water, but generally limited to the green EM spectral region to about 600 nm. This clearly indicates why a green pulse at 532 nm is very well suited for laser bathymetry from the air and is used in most ALB systems (for example SHOALS Guenther et al., 2000a, p. 16, 2000b, p. 16 and Hawk Eye II McNair, 2010, p. 25).

Besides being the frequency-doubled version of the conventional 1064 nm laser (Wojtanowski et al., 2008), the information above clearly indicates that this laser wavelength has a very good chance to maximally penetrate different water bodies, hit the bottom of the water body, and return an echo to the airborne receiver.

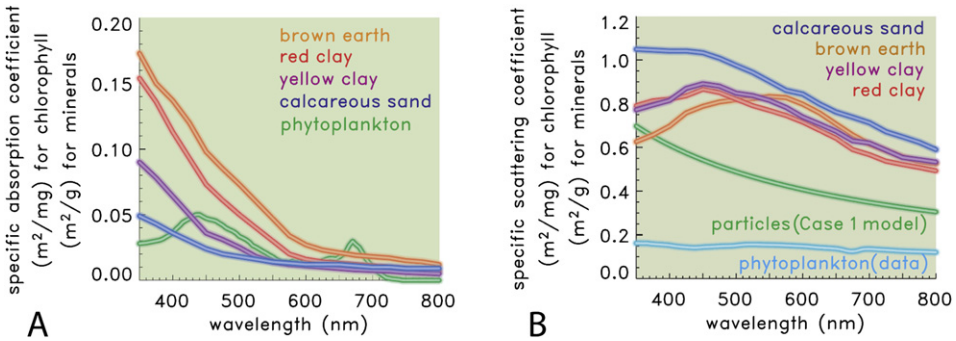

Fig. 2. A) Absorption coefficients (per unit mass concentration) and B) mass-specific scattering coefficients for different mineral particles and chlorophyll-rich phytoplankton (Figures from Mobley et al., 2004).

2.2. ALB history and operating principles

ALB is not an entirely new technique. Its first applications (detecting submarines) go back to the mid-1960s, shortly after the invention of the laser (Mandlburger et al., 2011, p. 2417). In the mid-1970s, several ALB prototypes were built and tested. At this time, the frequency-doubled laser systems with 532 nm pulses were also used (Kim, 1977). For an overview of the early historical development we refer to Guenther et al. (2000b, p. 3). Here, it is worthwhile mentioning that at the turn of the millennium several operating systems were available.

Similar to ALS, a bathymetric laser scanner is usually mounted below a fixed wing aircraft or helicopter, where it emits short green pulses towards the earth's surface (both water and terrain). Using various mechanisms (in our case a rotating mirror), the pulses are deflected in different directions across the flight path. Due to a beam divergence of the laser pulse, it will spread over a certain area, known as a footprint. Where it hits an object, a part of the energy (corresponding to the area of the footprint covered by the object and the object's reflectance) is backscattered, while the remaining portion of the pulse moves further on. In that way, each pulse will result in one or more echoes reflected from various objects along its path (vegetation, buildings, cars, ground surface etc.). The duration between pulse-emission and reception of the backscatter determines the laser-object distance. Together with the angle of the emitted laser beam and the position of the scanner (typically determined using a differential global navigation satellite system (GNSS) and an inertial measurement unit (IMU)), the location of each reflecting object is calculated (Doneus et al., 2008).

With ALB, the process is complicated by signal propagation in different optical media (air and water). When entering the optically thicker medium of water (air–water-interface) the green laser pulse is deflected and the propagation speed of EM radiation is reduced (Fig. 3). Whereas the propagation speed is entirely described by the refraction coefficient, the beam deflection is additionally influenced by the laser incidence angle. The former depends on the water body (its constituents, salinity and temperature), and the latter varies both due to the scan angle of the laser pulse and the roughness of the water surface. To keep the incidence angle constant (maximum deviation of $\pm 1^\circ$ over the entire scan range of 60° assuming a perfectly horizontal water surface), the laser pulses are tilted by 20° from the nadir direction. This results in a scan pattern in the shape of an arc of an ellipse (Mandlburger et al., 2011, p. 2418; for a detailed discussion of the nadir angle see Guenther et al., 2000a, 2000b, 10

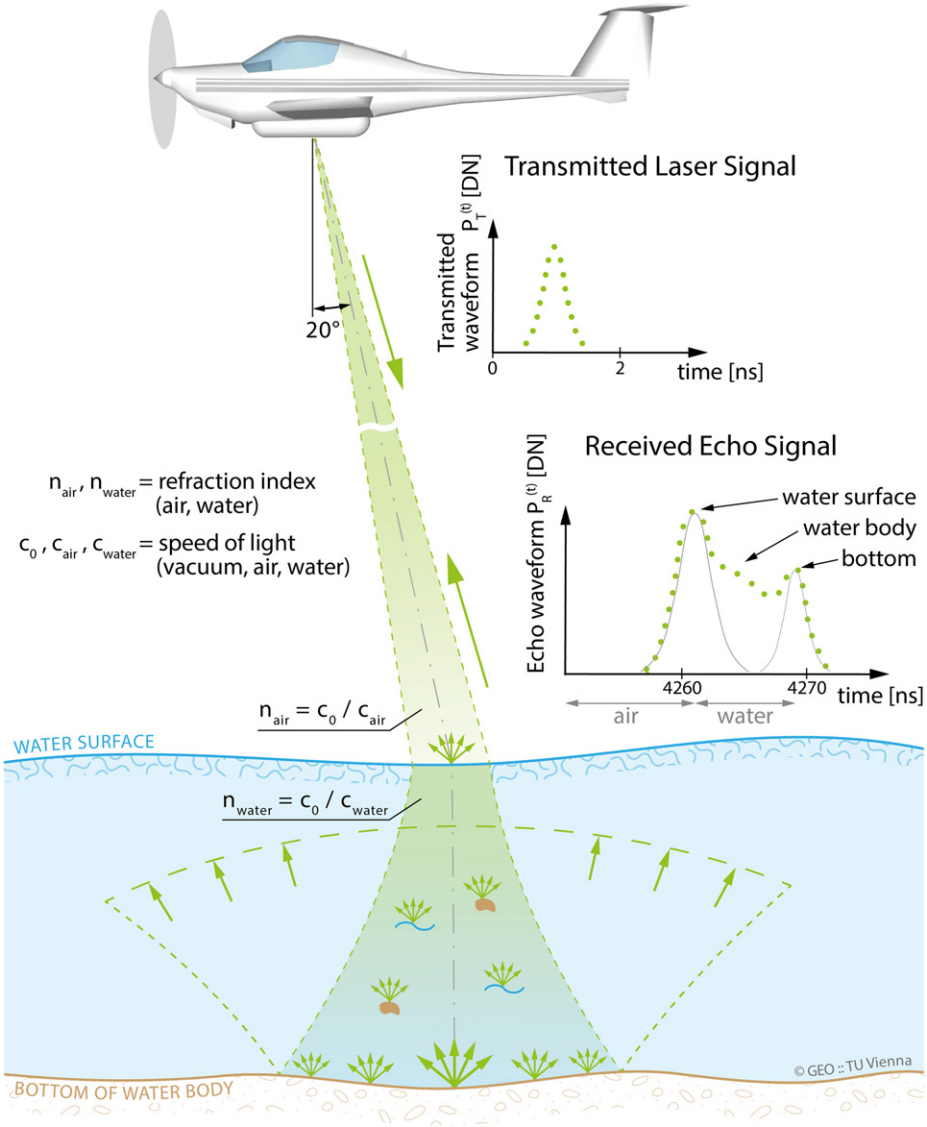

Fig. 3. Diagram explaining ALB. See text for further information (©Department of Geodesy and Geoinformation Research Group Photogrammetry, E120.7).

ff.). Additionally, the water surface has to be detected and modelled in post-processing to be able to correctly apply the refraction correction. Finally, the optical properties of water further spread the laser beam to such an extent that the backscattered laser echo can no longer be described by a simple Gaussian shape (Mullen, 2009; Cochenour et al., 2008). Depending on the water body, this scattering results in an overall loss of water-leaving radiance and in radiation directions that cannot be observed by the receiver. As a consequence, the illuminated portion of the bottom increases as does the uncertainty in depth estimation (Kunz et al., 1992).

So far, available ALB systems are designed for maximum penetration of water bodies using long (~7 ns) and high energy (~5 mJ) laser pulses with a typical pulse repetition rate of approximately 1 kHz. For eye safety reasons, the green laser beam has to be spread to a footprint diameter of several metres. This results in ground sampling distances of 2–5 m at typical flying heights between 200 and 500 m (Guenther et al., 2000b, pp. 3–5). Since the maximum survey-depth mainly depends on water clarity, it is usually specified in Secchi depths. This is an empirical water clarity measure denoting the depth at which a 20 cm wide black and white disc is just perceptible. Current ALB systems can survey under-water distances between 2 and 3 Secchi depths. Depending on the clarity of water, this can equal a depth of 50 m and more (Guenther et al., 2000b, p. 5; Wojtanowski et al., 2008).

Long pulses, relatively low repetition rates, wide footprints, and comparatively deep water penetration make current ALB systems viable tools for providing topographic models of coastal waters (Cunningham et al., 1998; Wozencraft and Millar, 2005; Allouis et al., 2010), lakes and shallow continental water (Hilldale and Raff, 2008) with a planar grid spacing of a few metres. Investigating the reflectance of the individual laser echoes provides additional information to classify the degree of vegetation (Wang and Philpot, 2007) or hydrodynamic processes (Long et al., 2010). So far, ALB has been used for archaeological purposes on the Black Sea Coast in Bulgaria (Prahov et al., 2011), where the underwater surface model was used as a component for predictive modelling. A combined use of ALB with side-scan sonar within the Irish National Seabed Survey to investigate areas with "high archaeological potential" is also mentioned (Lambrick, 2008, 56).

2.3. The Riegl ALB system

Although their spatial resolution would be useful to visualise and investigate submerged landscapes (e.g. Westley et al., 2010), current ALB systems would not meet the criteria specified for the archaeological research in this paper. Therefore, the recently designed novel hydrographic laser scanner RIEGL VQ®-820-G, manufactured by RIEGL Laser Measurement Systems GmbH in cooperation with the University of Innsbruck Unit of Hydraulic Engineering, was tested (Riegl, 2012).

The innovative aspects of the instrument are (i) its light-weight design (25 kg), (ii) high effective measurement rate (200 kHz), and (iii) the utilization of very short laser pulses (approximately 1 ns) and (iv) integrated online waveform processing. The moderate weight makes the instrument particularly suitable for mounting in helicopters and light-aircraft, allowing flexible flight paths. The high measurement rate yields a point density of up to 50 soundings per square metre depending on the flying height, and the short pulses enable the measurement of extremely shallow water depths (in the range of 20 cm). With 1 mrad, the instruments beam divergence is wider compared to topographic ALS systems (0.2–0.5 mrad) due to eye safety reasons. This results in a footprint diameter of 0.5 m at a flying height of 500 m. Altogether, this results in a reduced water penetration capability of about 1 Secchi depth.

The returning echo waveform is digitised with an interval of less than 1 ns and can be either processed online (online waveform processing – see Pfennigbauer and Ullrich, 2009) or stored and post-processed (full-waveform processing – see Hug et al., 2004). Similar to ALS, full-waveform analysis results in additional physical parameters which can be utilised to improve the quality of the resulting DTM and enhance interpretation (e.g. Wang and Philpot, 2007). However, the current capacity for storing the full waveform information is restricted by the internal data buffer of the scanner.

3. Case study

To test the capabilities of the new ALB system for archaeological purposes, a flight mission was arranged over selected case study areas. One of these, the small island of Sveti Petar demonstrates the archaeological potential of this new scanning system.

3.1. The island of Sveti Petar

Sv. Petar is located on the northern Croatian Adriatic coast, 2 km southwest of the Island of Lošinj (Fig. 4), separated from the island of Ilovik by a 200–400 m wide channel. The maximum extents of the island are roughly 2000 by 700 m. Altogether, it occupies an area of 94 ha. Its highest elevation is a roughly 64 m high hill in the south. The geology is comprised largely of limestone, densely covered with typical Mediterranean vegetation consisting mainly of dense, rigid, mostly evergreen shrubbery (macchia). In some areas, abandoned and recently used olive tree plantations can be found, which are enclosed by dry stone walls. Pine trees are mainly confined to the coastal areas (Fig. 5a and b).

Macchia, which is anthropogenic secondary vegetation, and a system of dry stone walls covering most of the island are indicators of past intensive human utilization, although the island is uninhabited today. The advantages of the natural harbour between Sv. Petar and Ilovik, which offers protection from most winds, were recognized from an early date and the small island was already populated in prehistory (Ćus-Rukonić, 1982, 12). More prominent sites on the island are a monastery and church of Saint Peter dating back to the 11th century, which houses the present-day cemetery of Ilovik, and a late 16th century Venetian fortification (Fig. 5c) (Fučić, 1949, 74 ff.). The focus of the test scan was, however, a large Roman settlement complex. The remains are located on the southern coast of Sv. Petar, opposite the village of Ilovik (Fig. 6). A high quantity of ceramics, graves, and architectural details as well as widespread building material demonstrate the importance of this Roman site (Fučić, 1949, 74; Čaušević-Bully and Bully, in press).

The remains of Roman buildings have been located both on land and in the sea. This makes the site interesting for our research – due to the changing seawater level of the Mediterranean during the last 1500 years large building sections have become submerged. The degree and rate of sea-level rise are still a matter of debate (suggestions range from 1.5 to 3.1 m – Faivre et al., 2011, p. 132). Submerged archaeological remains and tidal notches indicate a regionally varying sea-level at around 1.5 m below present mean sea-level during Roman times (Antonioli et al., 2007; Faivre et al., 2010). Therefore, archaeological coastal sites are at least partially located under water. As a result, at several locations over a length of 300 m remains of walls continuing into the water can be identified (Fig. 5d). The height difference between the surface of the walls and the surrounding area is however minimal (between 5 and 20 cm). It was therefore uncertain whether the ALB-derived DTM would be precise enough to visualise them.

3.2. Data acquisition

The test flight was conducted by Airborne Technologies (ABT) on 29th of March 2012 between 10:54 and 11:33 local time. Wind and water conditions were calm. The flying height was approximately

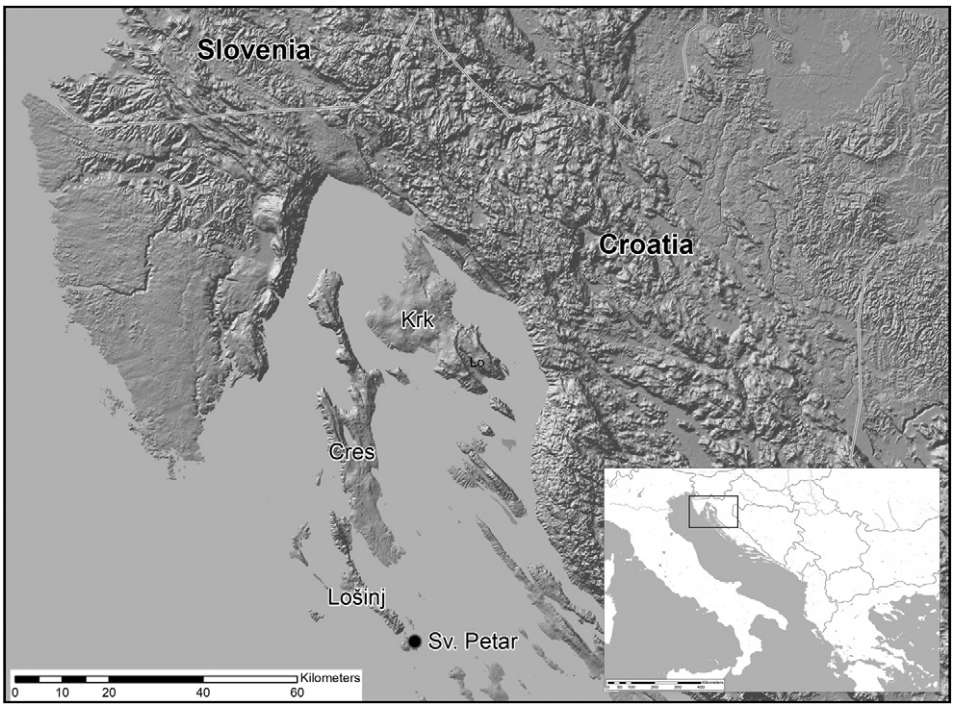

Fig. 4. Map of the northern Adriatic coast indicating the location of the island of Sv. Petar. Data Source: SRTM. North is up.

Fig. 5. Ground photographs of Sv. Petar; (a) macchia overgrowing a dry stone wall (b) olive tree from a former plantation (c) Venetian fortification (d) wall of a Roman villa continuing into the water.

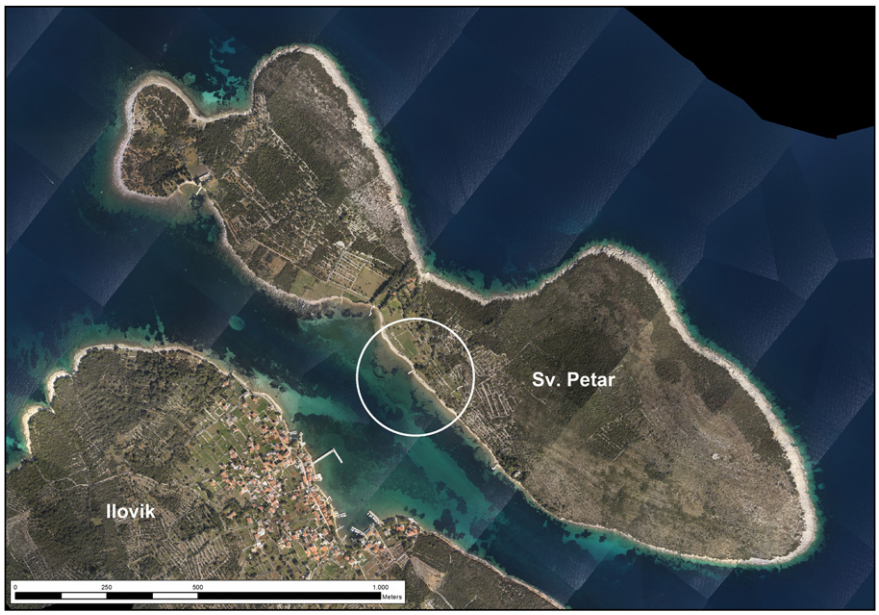

Fig. 6. Mosaic of orthophotographs from March 2012 of Sv. Petar indicating the location of the case study area presented in this paper. North is up.

450 m above ground level, which resulted in footprints of 0.45 m diameter on the water surface. The effective measurement rate was approximately 200 kHz. To guarantee eye-safety, the low energy mode, with a special instrument setting provided by RIEGL, was used. The scan angle was set to the full field of view of the instrument (60°). According to Mobile Geographics (http://tides.mobilegeographics.com/calendar/year/3554.html), which utilizes the software Xtide (http://www.flaterco.com/xtide/tty.html), low tide occurred on March, 29 at 7:49 while high tide was at 23:25. This means that the data acquisition took place at low tide conditions (the maximum tidal range is 61 cm).

Altogether, 9 longitudinal strips with an overlap of 70% and one cross-strip were acquired. Echo detection was realized using the scanners online waveform processing capability (see Pfennigbauer and Ullrich, 2009). The data were processed by ABT, using the software RiPROCESS. This resulted in a total point cloud (including all echoes) with a density of 10–50 points per square metre (Fig. 7).

As discussed above, deriving the range between scanner and sub-water surface and assigning coordinates to the reflecting objects is difficult. Calculating the range and refraction correction due to signal propagation in air and water requires a good model of the contemporaneous conditions and shape of the water surface, as the speed of light differs for atmosphere and water. While the system used provided good initial results, especially over land, remaining systematic errors between the strips stemming from a too simple model of the water surface could be minimized using least squares

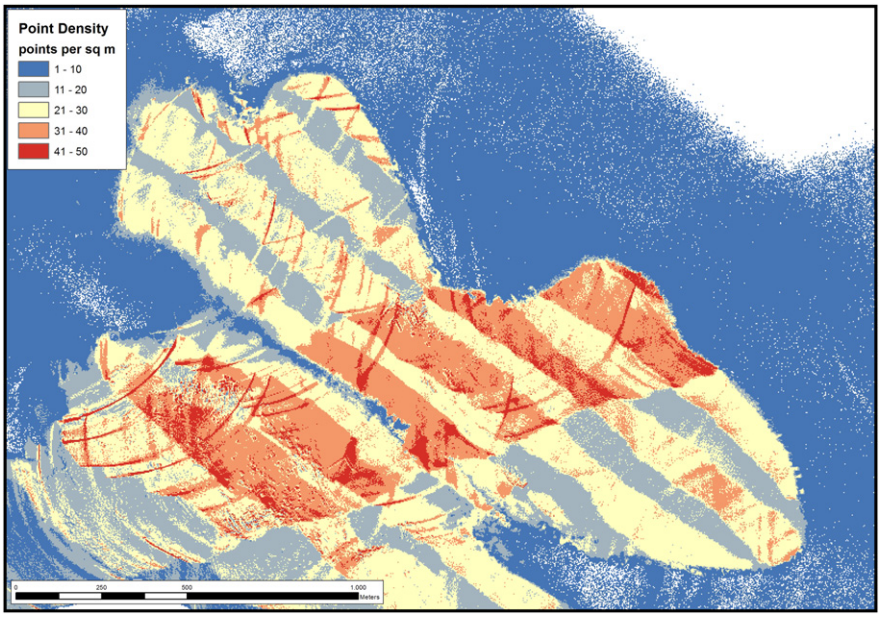

Fig. 7. Colour-coded distribution map showing the point density of the ALB scan (resolution = 1 m). On land, the point density is quite high (10–30 points per square metre). Especially in the area covered by an additional cross-strip, it reaches up to 50 points. Over water, the point density decreases with water depth (compare Fig. 9). Note the arc-pattern which is a result of the tilted laser beam direction (20° from nadir). North is up. (For interpretation of the references to colour in this figure legend, the reader is referred to the web version of this article.)

matching of overlapping strip pairs and a subsequent least squares adjustment of the entire flight block (Ressl et al., 2009). Strip adjustment (Fig. 8) was accomplished utilizing the software package OPALS (Mandlburger et al., 2009).

The strip adjusted last echo point cloud still contains a substantial number of off-surface points (one should never forget that the returning waveform is an integration of the sea floor, water column and water surface signatures – Collin et al., 2008). These will be predominantly due to gross errors (e.g. multi-path) and systematic errors (e.g. some points will be from buoys, ships, fish or dense vegetation) and have to be reduced by employing advanced filter methods. In this case, the technique of robust interpolation with an eccentric and asymmetrical weight function was used (see Doneus et al., 2008, p. 887). The remaining point cloud was finally imported into a GIS environment for further visualisation and interpretation. There is already abundant literature regarding archaeological visualisation of ALS-derived DTMs (Bennett et al., 2012; Challis et al., 2011; Devereux et al., 2008; Hesse, 2010; Kokalj et al., 2011). In this study, hillshade, slope, local relief model (Hesse, 2010) and positive as well as negative openness (Yokoyama et al., 2002) were calculated and used both exclusively and in various combinations.

3.3. Results

The resulting DTM combines land surface and underwater topography. As was to be expected, filtering the dataset resulted in a point cloud with a varying point density (Fig. 11). While the process of robust interpolation did not remove many points on the often bare underwater surface, the point density was highly reduced in the densely vegetated areas of the islands. Particularly, macchia prevented a high number of pulses from reaching the ground surface. This situation was additionally aggravated by the fact that the tilted scan direction resulted in longer travel paths of the individual pulses through the vegetation. On the islands of Sv. Petar and Ilovik the dense Mediterranean vegetation could be removed completely by the applied filter algorithm, but due to the low number of ground points the resulting terrain model shows

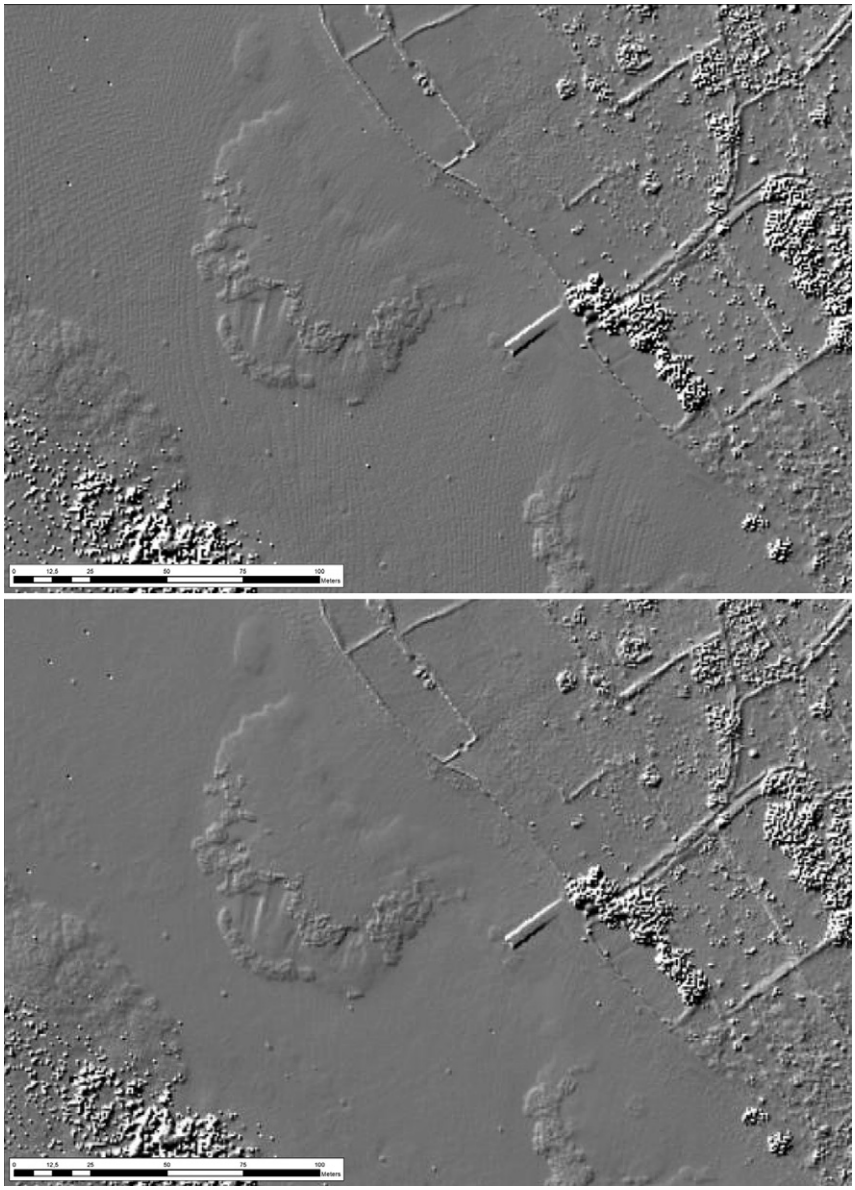

Fig. 8. Point density map of DTM derived from the unfiltered last echo point cloud from the case-study area in Sv. Petar without (upper image) and with (lower image) strip adjustment. North is up.

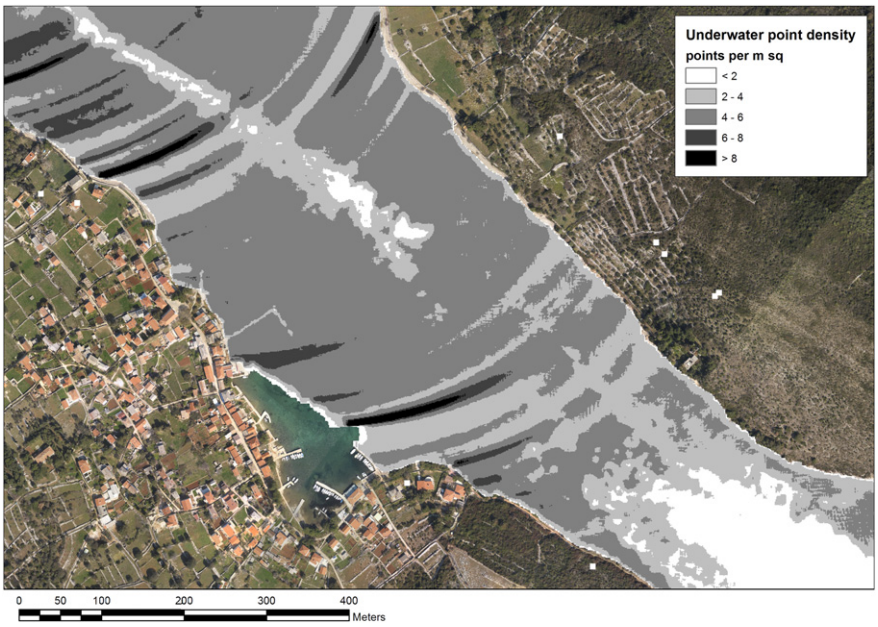

Fig. 9. Orthophotograph of the channel between the islands of Ilovik and Sv. Petar overlain with a grey-coded distribution map of underwater point density (resolution = 1 m). In the extremely shallow zone (i.e. <0.2 m) at the transition between land and water, the point density is low (due to problems of echo separation). At water depths between 0.2 m and 6.5 m, the point density varies only due to nick-movements of the airplane (arc-shaped under- and overscan). In the centre of the channel, the point density decreases at water depths below 6.5 m. North is up.

little detail (Fig. 11). However, the system of dry stone walls becomes clearly visible. More importantly, the terrain model of the underwater surface displays high detail up to a water depth of approximately 8 m (Fig. 9). Due to the high initial point density and the minor loss of points after filtering, a digital model of the underwater topography with a grid spacing of 25 cm could be derived (Fig. 10). As a result, the channel dividing Sv. Petar from Ilovik could be covered almost entirely; only a few small areas were deeper than the maximum penetration depth of the scanner system.

Fig. 11 displays the area of the Roman villa. A colour-coded map of the water depth is superimposed on the shaded DTM. The Roman site can be recognised by the large amount of pottery that can be found along the shoreline and a few walls within the small intertidal zone (Fig. 5d). Interestingly, the DTM reveals a submerged 80 by 60 m platform. According to the cross-section, it is more or less horizontal (Fig. 11A and B). The height difference to the surrounding sea floor is 1 m in the north and 2 m in the south. Coming from the island, the terrain drops slightly by 1 m over a length of 20 m until it reaches the platform, which has an almost flat convex surface and slopes by 0.4 m over a length of 40 m, before it falls off by almost 2 m to the sea floor (Fig. 11, Profile C and D).

The hillshade already indicated some possible linear structures within the area of the platform. However, due to the minor difference in elevation (see also Fig. 5d), more sophisticated

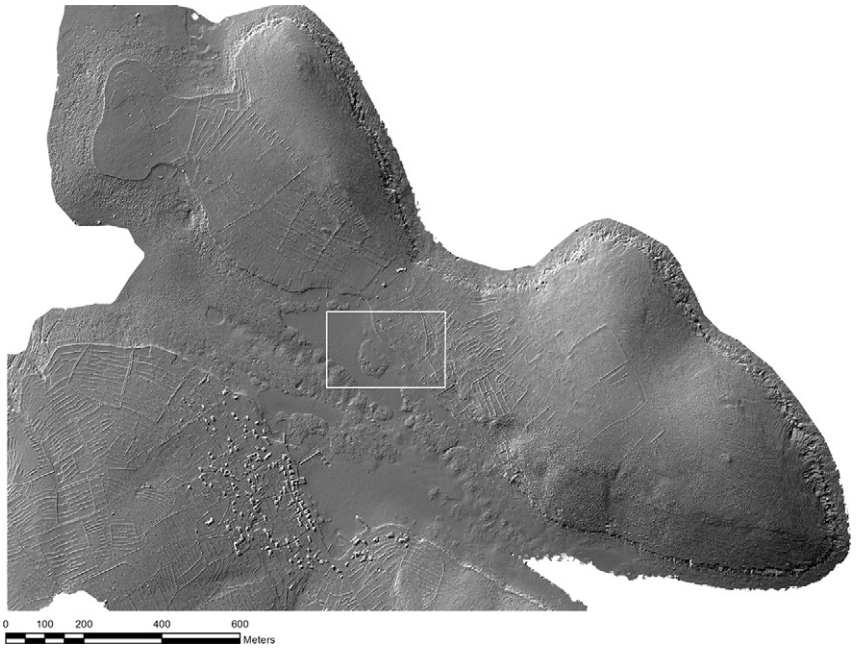

Fig. 10. Sv. Petar. ALB-derived, shaded digital terrain model after robust interpolation. The white rectangle marks the outline of Fig. 11. North is up.

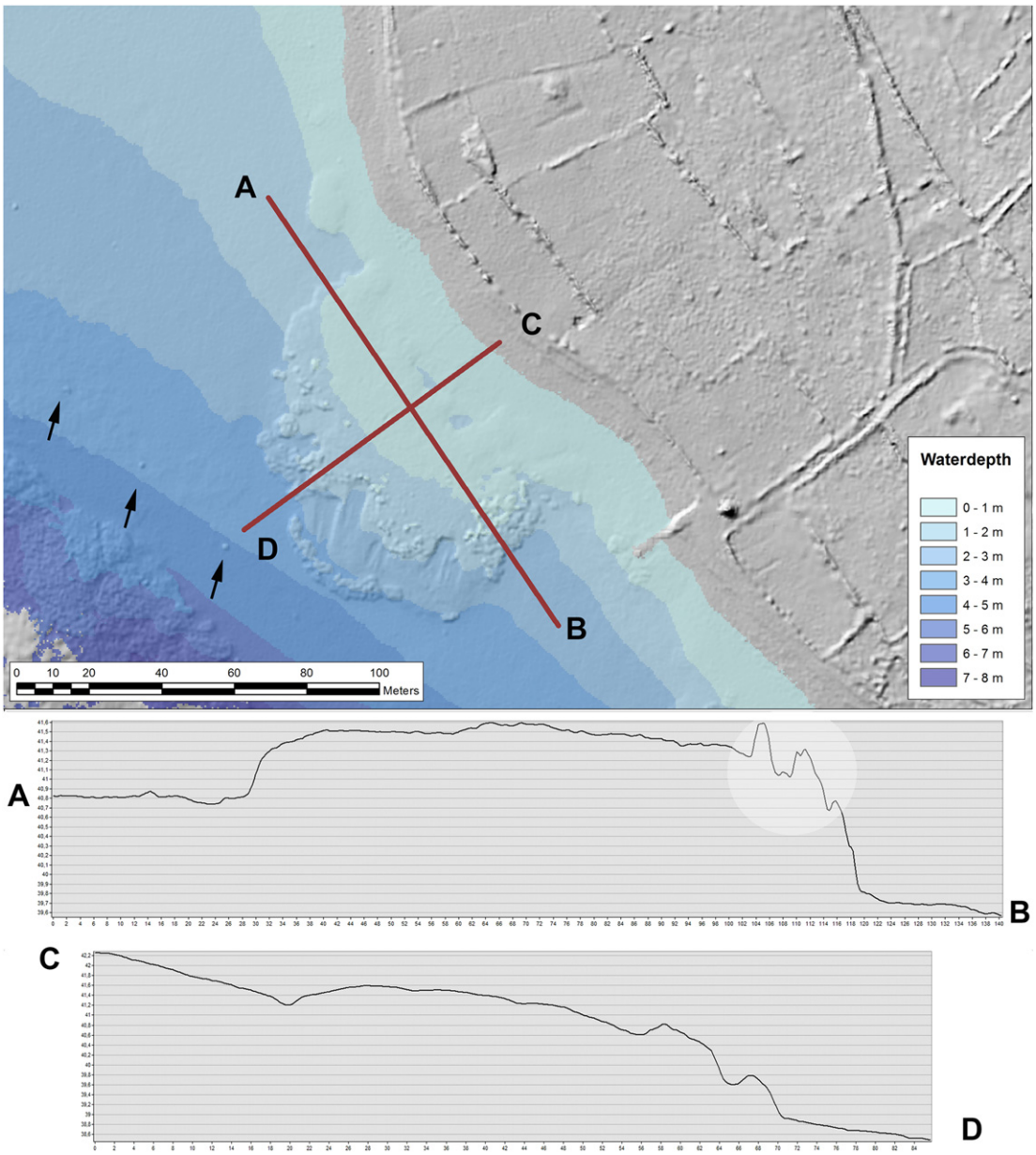

Fig. 11. Shaded filtered DTM superimposed with a colour-coded map of the water depth generated from the ALB data acquisition campaign over the Roman villa site. The shaded DTM combines land surface and underwater topography. Arrows point at individual anchoring stones for buoys. The cross-section A–B shows a more or less even, raised platform with the spikes highlighted in the light circle due to seagrass, which was not removed by the filter algorithm. Cross-section (A–B): 2 m height, 140 m width. Cross-section (C–D): 3.5 m height, 85 m width. North is up. (For interpretation of the references to colour in this figure legend, the reader is referred to the web version of this article.)

visualisation techniques had to be utilized. Most promising was the local relief model (LRM; Hesse, 2010) where the detailed DTM is subtracted from its low-pass filtered derivative resulting in a relief model which enhances micro-topography. The degree of enhancement depends on the kernel size of the low-pass filter, which has to be adapted to the size and degree of relief variation within both the terrain and its micro-topographic structures. After systematic testing, a kernel size of 10 m yielded the best results in our case study (Fig. 12). The LRM was colour-coded with raised features (stones, walls, seagrass) displayed in red and lowered areas in blue.

An inspection of the LRM displayed in Fig. 12 reveals several linear structures, as well as rectangular areas which are higher than the surroundings (compare with Fig. 13). With a few exceptions, the orientation is NE–SW and NW-SE respectively, i.e. the structures are parallel and perpendicular to each other. They can therefore be interpreted as walls and former floors of a building complex which were more resistant to erosion. Only four linear structures follow a deviating course, but again are set at right angles to each other. These seem to be related but it is uncertain whether they are from a different chronological phase. In most cases the walls are 1 m broad and show height differences to the surrounding sea floor between 5 cm and 15 cm. The floors are often raised by 15–20 cm.

This interpretation could be verified on-site at the end of July 2012. During two visits at high tide, the area was documented using an underwater camera (Canon PowerShot D20) while snorkelling. Some of the walls could be easily recognised (Fig. 14) and photographed. Others were covered with mud and algae and therefore very hard to identify. At all locations, the water column was a maximum of 1.5 m, while predominantly pottery could be found on most of the platform area.

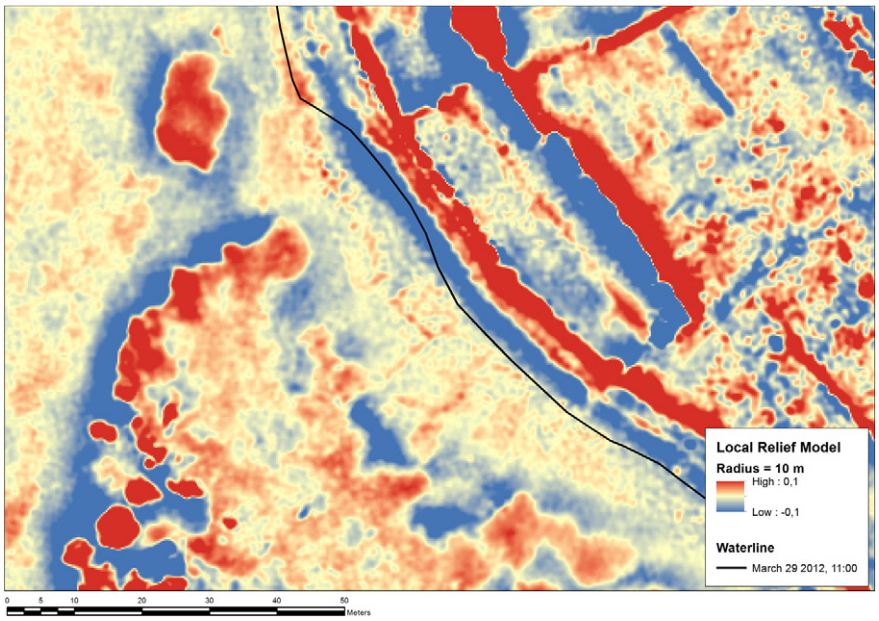

Fig. 12. The local relief model of the submerged platform reveals raised linear structures and rectangular areas (in red). Kernel-size of the low-pass filter was 10 m. North is up.

4. Discussion

The results clearly demonstrate that ALB has the capability to shift the measurement border from the water-land boundary into the water. This allows for the inclusion of shallow-water zones, which can otherwise hardly be mapped in detail, into topographic documentation. This is important since, until now, archaeology lacked suitable methods to provide detailed maps of the topography of these extremely shallow underwater bodies.

Theoretically, digitising submerged structures in the first 25 cm of the water column can be problematic if an individual laser pulse is reflected both from the water surface and the sea floor (see also Fig. 9). In this case echo separation would not be possible since the minimum discrimination range lies at about 25 cm (Mandlburger et al., 2011, p. 3422). This could result in more noise within this area. From a visual inspection of the resulting DTM and the cross section through the point cloud, this problem seems not to be relevant in our case study. This could be due to the fact that in many cases, laser pulses are not reflected from the water surface but only provide a sea floor echo.

As mentioned above, the penetration depth of the bathymetric laser scanner is a compromise between footprint size (narrow laser beam allowing for an increased resolving power) and high laser energy (allowing deeper water penetration) due to eye-safety reasons. A small footprint size is a necessity to yield high resolution DTMs. In combination with the high repetition rate and a 50% overlap between adjacent flying strips, a spatial resolution of 25 cm could be achieved in Sv. Petar. This is high enough to visualise even individual larger stones at a depth of several metres. The arrows in Fig. 11 point to individual concrete anchor stones for buoys at

Fig. 13. Interpretation of the ALB derived data superimposed on the orthophotograph. The arrow roughly indicates the position of the photograph Fig. 14. North is up.

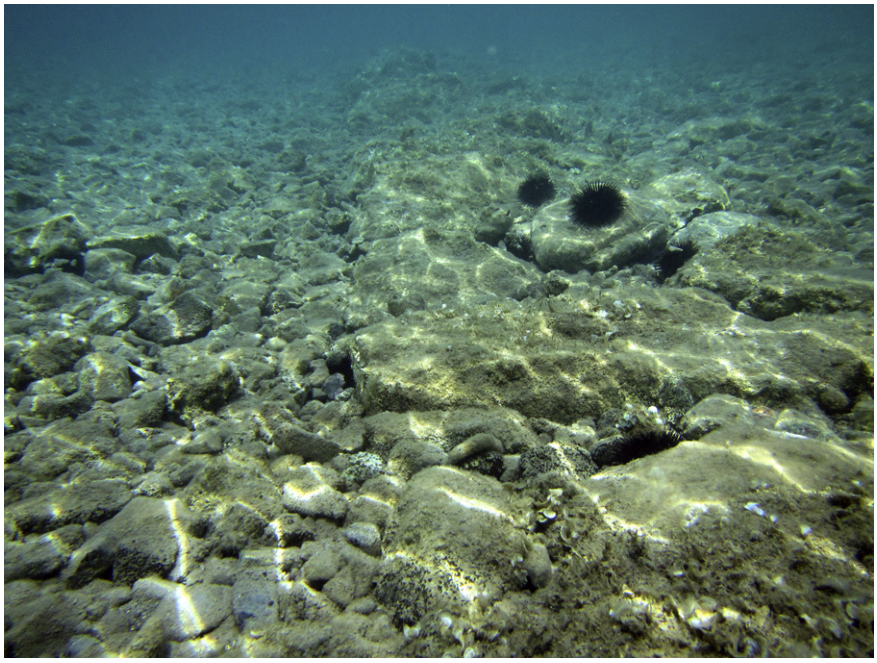

Fig. 14. Submerged wall (see arrow on Fig. 13 for approximate position) as photographed on July 22nd around 1 PM using a Canon PowerShot D20 underwater camera.

a depth of 4 m. This is a novelty, since the design of existing ALB systems only allows for grid sampling distances of several metres at a relatively high penetration depth.

High spatial resolution is, however, achieved at the expense of penetration depth, which depends on the water constituents and is specified as up to one Secchi depth. In our case study the maximum measurable water depth was 8.2 m. Anyway, we argue that with the exception of shipwrecks, a high percentage of the submarine archaeological structures will be situated within this depth range (at least in the Mediterranean).

The penetration depth of 8 m was achieved on a calm day and – documented by the simultaneously acquired vertical aerial photographs – over clear water with a relatively smooth water surface. These are ideal conditions for ALB data acquisition. The results can thus not be applied to other parts of the world. Consequently, testing the validity of the method in different aquatic environments is one of the future research topics. A recent scan over the turbid Austrian Keutschacher See confirms the instrument's specification that the penetration equals 1 Secchi depth, which in this case was 1.6 m. This, however, was enough to map the topography of a shallow Bronze Age lake dwelling located in the lake's centre.

Besides environmental conditions such as water depth, surface roughness and water clarity, the sea floor type also has an important impact on the quality of the ALB dataset. Submerged aquatic vegetation can be especially problematic. In Sv. Petar, several areas are overgrown with seagrass (Fig. 15) which is very dense and was

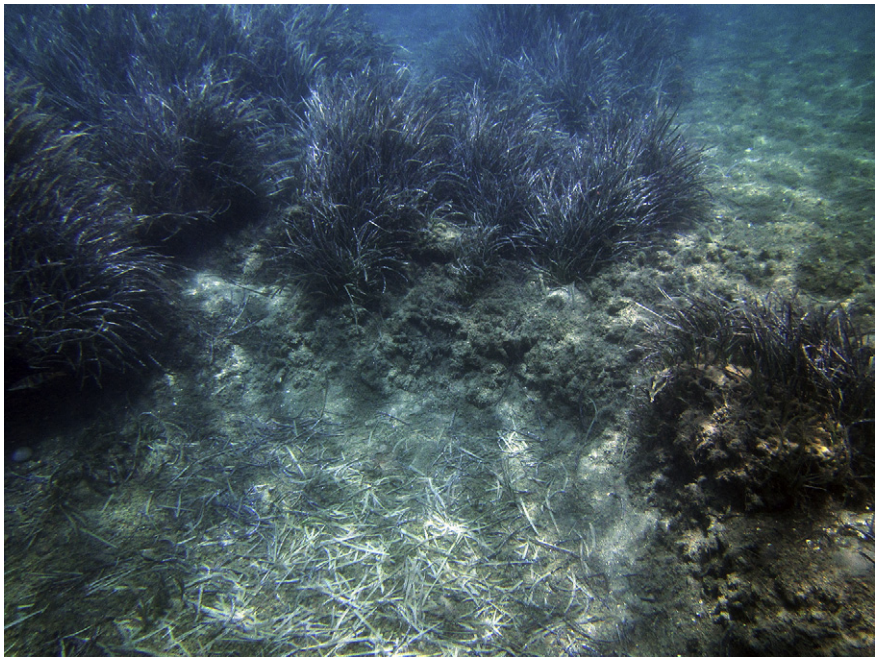

Fig. 15. Seagrass photographed on July 22nd around 13:00 using a Canon PowerShot D20 underwater camera.

not removed by the filter used for our case study (Fig. 16). Further experiments are needed to study the ability of the ALB system to penetrate underwater vegetation. Storage of the entire waveform data, which is planned for the next generations of Q-820-G scanners, would enable more sophisticated signal analysis compared to the information obtained from the current online waveform processing results. Given certain underwater vegetation penetrability, advanced filtering techniques taking additional waveform parameters into account (e.g. amplitude or pulse deviation) could be helpful in these areas (compare Doneus and Briese, 2006).

Some of the submerged walls are also visible on the aerial photographs, which were acquired simultaneously with the ALB scan. This is due to the fact that they are located in shallow, smooth and very clear water. Besides, the walls that are discernible in the vertical air photo consist of large stones which produce a good visual contrast with the surrounding sea floor. In other areas with less pronounced contrast, the walls are invisible in the photographs, but were still recorded in the ALB-derived DTM (Fig. 17). Using the local relief model, very small elevation differences (between 5 cm and 20 cm) could be visualised. As an active system ALB is also sun angle independent (i.e. no issues with reflections and glint) and is not disturbed by shadowed areas (Hilldale and Raff, 2008), giving it an additional edge over passive optical imaging (although the latter provides colour information).

Besides the fact that it is useful for extremely shallow water, one other major advantage of ALB compared to other bathymetric methods (mainly different versions of sonar – sound navigation and ranging) is the short acquisition time needed. This is mainly due to the fact that, in contrast to sonar systems, in ALB the swath width is independent of the water depth and only depends on the flying height. Within just 40 min, an area of 10 square kilometres was covered with a high point density in Sv. Petar (see Fig. 7), resulting in a terrain model with a planar spatial resolution of 25 cm. ALB could thus be used over large areas for a rapid

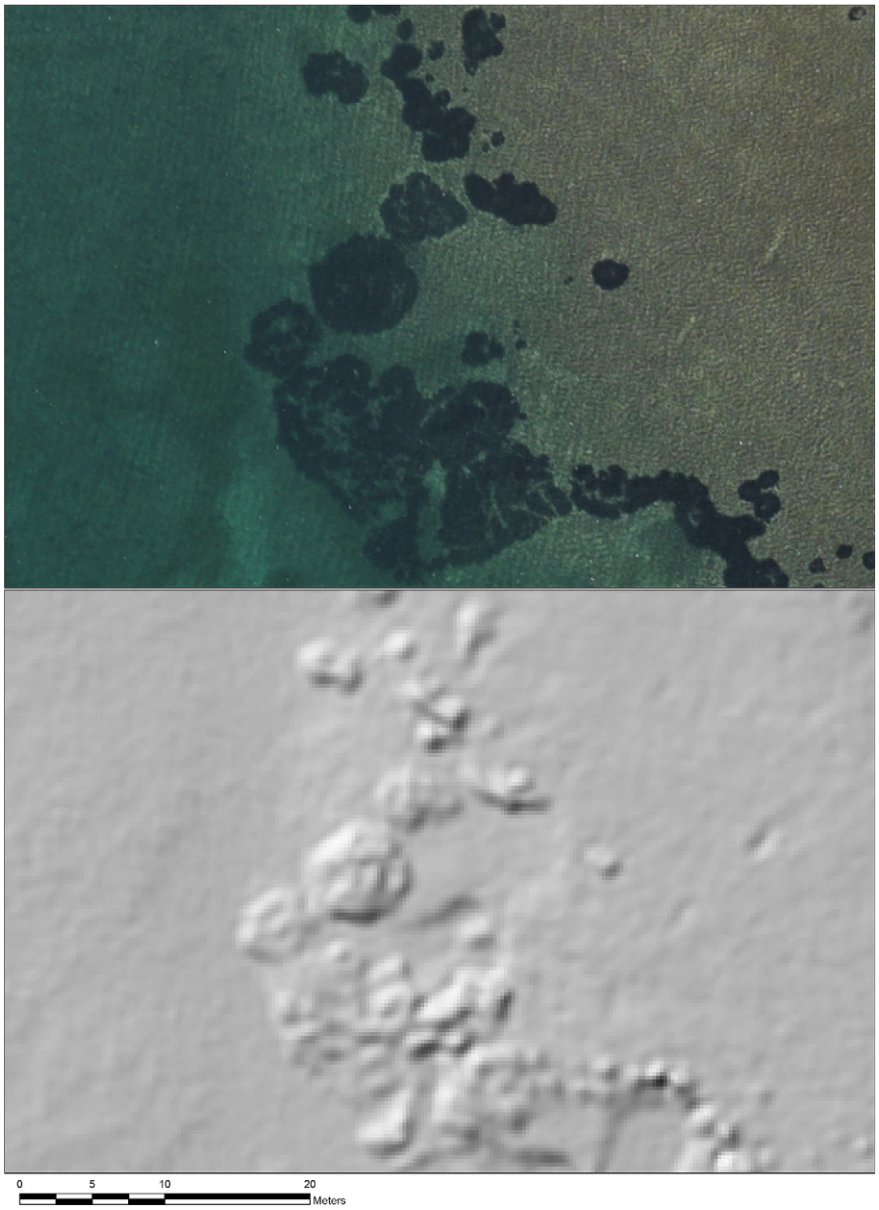

Fig. 16. Sv. Petar. Upper image: orthophotograph of an area partly covered with seagrass (dark green). Lower image: shaded DTM of the same area after filtering. The dense seagrass was not removed by the filter algorithm. North is up. (For interpretation of the references to colour in this figure legend, the reader is referred to the web version of this article.)

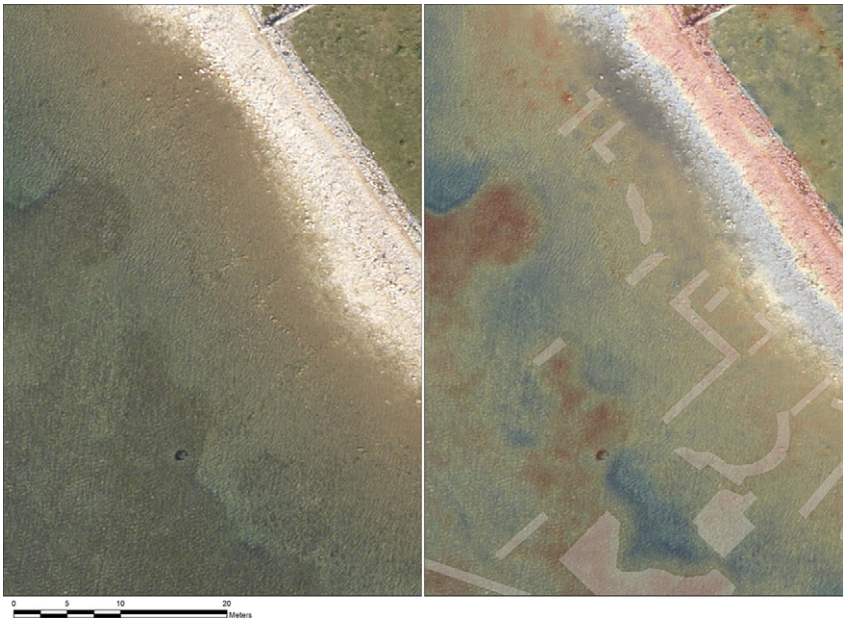

Fig. 17. Left: Orthophotograph of the Roman villa. Some walls are clearly visible. Right: superimposed with a LRM and an interpretation drawing. North is up.

assessment of potential archaeological traces and topographical features, while any detailed information can subsequently be gathered using sonar in smaller predefined areas, an integration already proposed by Danson (2006).

As with sonar and ALS, only archaeological sites and structures still surviving in (micro-) relief can be visualised and identified. Buried features or sites, which do not have relief traces, cannot be detected in an ALB-derived topographic model. Also, a high quality DTM is necessary in order to be able to interpret individual archaeological structures.

The quality of the DTM is determined by various factors, most importantly point density (see Fig. 9, which determines the final spatial resolution of the DTM) and the quality of water surface modelling (which has an effect on the correct geolocation of the scatterers for each laser echo). Additionally, the successful removal of all object points which do not belong to the ground surface is necessary. On the land, vegetation removal is slightly complicated by the tilted scan angle. Travel distances of a laser pulse through dense vegetation is hereby extended, which reduces the chance that the last echo is actually returning from the ground surface. To digitally remove dense submerged aquatic vegetation would require filter settings that could potentially also remove archaeological structures. To what extent the inclusion of additional attributes derived from the full waveform signal can enable a more advanced filtering approach remains to be researched.

5. Conclusion

The paper has demonstrated that the recent development of a green laser with narrow footprint and short repetition rate is able to provide topographic data of both land surfaces and shallow-water zones. Unlike existing ALB systems, it can yield very detailed terrain data at better than 1 m planimetric spatial resolution. This is due to the small beam divergence of the laser (1.0 mrad), resulting in narrow footprints (in our case with a diameter of 0.45 m at a flying height of 450 m) combined with a high effective measurement rate of about 200,000 measurements per second.

Using a case study area of a submerged Roman villa on the northern Croatian Adriatic coast, the archaeological potential of this new scanning system is demonstrated. The flight pattern, which allowed for a more than 50% overlapping area of adjacent scanned strips at the previously-mentioned small footprint size, resulted in an underwater DTM with cell sizes of less than 1 m. The spatial resolution was high enough to visualise several walls and floors of the villa complex exhibiting height differences between 5 cm and 20 cm, which are located under a water column between 0 m and 1.5 m. Even larger individual stones in water depths of several metres could be spatially resolved.

For the first time, large-scaled shallow-water zones can now be measured systematically in detail. This is important since, until now, archaeology has lacked suitable methods to provide detailed maps of the topography of these (extremely) shallow underwater bodies. What is also important is the fact that the result of ALB is a topographical model both of the area under shallow water and that above the water level. Therefore, coastal areas can be mapped in their entirety using a single method.

We anticipate this technique also as a major break-through in further scientific fields which are in need of detailed topographic maps of intertidal zones and shallow-water bodies. Furthermore, multi-temporal ALB missions could reveal environmental change by documenting underwater sedimentation and erosion rates, as well as changes in underwater vegetation. In the field of archaeology the results will have an important impact as, with the exception of shipwrecks, underwater archaeology often deals with submarine archaeological structures that are located in these shallow-water zones.

Acknowledgements

The flight was funded by RGZM Mainz in preparation of the project “Harbours and landing places on the Balkan coasts of Byzantine empire (4.–12. Century). Technology and monuments, economic and communication.”

The Ludwig Boltzmann Institute for Archaeological Prospection and Virtual Archaeology (archpro.lbg.ac.at) is based on an international cooperation of the Ludwig Boltzmann Gesellschaft (A), the University of Vienna (A), the Vienna University of Technology (A), the Austrian Central Institute for Meteorology and Geodynamic (A), the office of the provincial government of Lower Austria (A),

Airborne Technologies GmbH (A), RGZM-Roman-Germanic Central Museum Mainz (D), RA-Swedish National Heritage Board (S), IBM VISTA-University of Birmingham (GB) and NIKU-Norwegian Institute for Cultural Heritage Research (N).

The authors finally wish to express their thankfulness to the valuable comments of four anonymous reviewers.

References

Allouis, T., Bailly, J.-S., Pastol, Y., Le Roux, C., 2010. Comparison of LiDAR waveform processing methods for very shallow water bathymetry using Raman, near-infrared and green signals. Earth Surface Processes and Landforms 35, 640–650.

Antonioli, F., Anzidei, M., Lambeck, K., Auriemma, R., Gaddi, D., Furlani, S., Orrù, P., Solinas, E., Gaspari, A., Karinja, S., Kovačić, V., Suracel, L., 2007. Sea-level change during the Holocene in Sardinia and in the northeastern Adriatic (central Mediterranean Sea) from archaeological and geomorphological data. Quaternary Science Reviews 26, 2463–2486.

Bennett, R., Welham, K., Hill, R.A., Ford, A., 2012. A comparison of visualization techniques for models created from airborne laser scanned data. Archaeological Prospection 19, 41–48.

Blondel, P., 2009. The Handbook of Sidescan Sonar. In: Springer Praxis Books. Springer-Verlag Berlin Heidelberg, Berlin, Heidelberg.

Bowens, A. (Ed.), 2009. Underwater Archaeology: the NAS Guide to Principles and Practice, second ed. Blackwell Pub, Malden, MA, Oxford, p. 30.

Bukata, R.P., Jerome, J.H., Kondratyev, K.Y., Pozdnyakov, D.V., 1995. Optical Properties and Remote Sensing of Inland and Coastal Waters. CRC Press, Boca Raton, 362 pp.

Carbonneau, P.E., Lane, S.N., Bergeron, N., 2006. Feature based image processing methods applied to bathymetric measurements from airborne remote sensing in fluvial environments. Earth Surface Processes and Landforms 31 (11), 1413–1423.

Challis, K., Forlin, P., Kincey, M., 2011. A generic toolkit for the visualization of archaeological features on airborne LiDAR elevation data. Archaeological Prospection 18, 279–289.

Cochenour, B.M., Mullen, L.J., Laux, A.E., 2008. Characterization of the beam-spread function for underwater wireless optical communications links. IEEE Journal of Oceanic Engineering 33 (4), 513–521.

Collin, A., Archambault, P., Long, B., 2008. Mapping the shallow water seabed habitat with the SHOALS. IEEE Transactions on Geoscience and Remote Sensing 46 (10), 2947–2955.

Crutchley, S., Crow, P., 2010. The Light Fantastic: Using Airborne Lidar in Archaeological Survey. English Heritage Publishing, Swindon.

Cunningham, A.G., Lillycrop, W.J., Guenther, G.C., Brooks, M.W., 1998. Shallow water laser bathymetry: accomplishments and applications. In: Oceanology International 98 Conference Proceedings. The Global Ocean. Spearhead Exhibitions Ltd, pp. 277–288.

Curcio, J., Petty, C., 1951. The near-infrared absorption spectrum of liquid water. Journal of the Optical Society of America 41, 302–304.

Ćus-Rukonić, J., 1982. Arheološka topografija otoka Cresa i Lošinja (Archaeological topography of the islands of Cres and Lošinj). Izdanja Hrvatskog arheološkog društva 7, 9–17.

Čaušević-Bully, M., Bully, S. Sanctus Petrus de Nimbis (Ilovik), une station maritime majeure du nord de l'Adriatique, de l'Antiquité au Moyen-Âge. Histria antiqua 21, Pula, in press.

Danson, E., 2006. Understanding LiDAR bathymetry for shallow waters and coastal mapping. In: Shaping the Change. Proceedings of the XXIII FIG Congress, Munich, Germany. October 8–13, 2006.

Davies-Colley, R.J., Vant, W.N., 1987. Absorption of light by yellow substance in freshwater lakes. Limnology and Oceanography 32 (2), 416–425.

Dekker, A.G., Brando, V.E., Anstee, J.M., Pinnel, N., Kutser, T., Hoogenboom, E.J., Peters, S., Pasterkamp, R., Vos, R., Olbert, C., Malthus, T.J., 2002. Imaging spectrometry of water. In: van der Meer, F.D., de Jong, S.M. (Eds.), Imaging Spectrometry. Basic Principles and Prospective Applications. Remote Sensing and Digital Image Processing, vol. 4. Kluwer Academic Publishers, Dordrecht, pp. 307–358.

Devereux, B.J., Amable, G.S., Crow, P., 2008. Visualisation of LiDAR terrain models for archaeological feature detection. Antiquity 82, 470–479.

Doneus, M., Briese, C., 2006. Digital terrain modelling for archaeological interpretation within forested areas using full-waveform laserscanning. In: Ioannides, M., Arnold, D., Niccolucci, F., Mania, K. (Eds.), The 7th International Symposium on Virtual Reality. Archaeology and Cultural Heritage VAST, pp. 155–162.

Doneus, M., Briese, C., 2011. Airborne laser scanning in forested areas – potential and limitations of an archaeological prospection technique. In: Cowley, D. (Ed.), Remote Sensing for Archaeological Heritage Management. Proceedings of the 11th EAC Heritage Management Symposium, Reykjavik, Iceland, 25–27 March 2010. Occasional Publication of the Aerial Archaeology Research Group, vol. 3. Archaeolingua; EAC, Budapest, pp. 53–76.

Doneus, M., Briese, C., Fera, M., Janner, M., 2008. Archaeological prospection of forested areas using full-waveform airborne laser scanning. Journal of Archaeological Science 35, 882–893.

Engman, E.T., Gurney, R.J., 1991. Remote Sensing in Hydrology, first ed. Chapman and Hall; Van Nostrand Reinhold, London, New York.

Faivre, S., Fouache, E., Kovacic, V., Gluscevic, S., 2010. Geomorphological and archaeological indicators of Croatian shoreline evolution over the last two thousand years. GeoActa, Special Publication 3, 125–133.

Faivre, S., Fouache, E., Ghilardi, M., Antonioli, F., Furlani, S., Kovačić, V., 2011. Relative sea level change in western Istria (Croatia) during the last millennium. Quaternary International 232 (1–2), 132–143.

Firth, A., 2011. Marine geophysics: integrated approaches to sensing the seabed. In: Cowley, D. (Ed.), Remote Sensing for Archaeological Heritage Management. Proceedings of the 11th EAC Heritage Management Symposium, Reykjavik, Iceland, 25–27 March 2010. Occasional Publication of the Aerial Archaeology Research Group, vol. 3. Archaeolingua; EAC, Budapest, pp. 129–140.

Fučić, B., 1949. Izvještaj o putu po otocima Cresu i Lošinju. Ljetopis Jugoslavenske Akademije 55, 31–76.

Gitelson, A.A., 1992. The peak near 700 nm on radiance spectra of algae and water. Relationships of its magnitude and position with chlorophyll concentration. International Journal of Remote Sensing 13, 3367–3373.

Guenther, G.C., Brooks, M.W., LaRocque, P.E., 2000a. New capabilities of the "SHOALS" airborne lidar bathymeter. Remote Sensing of Environment 73, 247–255.

Guenther, G.C., Cunningham, A., Laroque, P., Reid, D., 2000b. Meeting the accuracy challenge in airborne lidar bathymetry. In: Workshop on Lidar Remote Sensing of Land and Sea. Proceedings of the 20th EARSeL Symposium, Dresden/FRG, June 16–17, 2000, Dresden, pp. 1–27.

Han, L., Rundquist, D.C., 2003. The spectral responses of *Ceratophyllum demersum* at varying depths in an experimental tank. International Journal of Remote Sensing 24 (4), 859–864.

Hesse, R., 2010. LiDAR-derived Local Relief Models – a new tool for archaeological prospection. Archaeological Prospection 17 (2), 67–72.

Hilldale, R.C., Raff, D., 2008. Assessing the ability of airborne LiDAR to map river bathymetry. Earth Surface Processes and Landforms 33 (5), 773–783.

Hug, C., Ullrich, A., Grimm, A., 2004. Litemapper-5600 – a waveform-digitizing LIDAR terrain and vegetation mapping system. In: Thies, M., Koch, B., Spiecker, H., Weinacker, H. (Eds.), Laser-scanners for Forest and Landscape Assessment. Proceedings of Natscan, Laser-scanners for Forest and Landscape Assessment – Instruments, Processing Methods and Applications, XXXVI. International Archives of Photogrammetry and Remote Sensing, vol. XXXVI, Part 8/W2, pp. 24–29.

Jensen, J.R., 2007. Remote Sensing of the Environment: an Earth Resource Perspective. In: Prentice Hall Series in Geographic Information Science, second ed., vol. xvi. Pearson Prentice Hall, Upper Saddle River, 592 pp.

de Jong, C.D., 2002. Hydrography, first ed.. In: Series on Mathematical Geodesy and Positioning DUP Blue Print, Delft, 353 pp.

Kim, H.H., 1977. Airborne bathymetric charting using pulsed blue-green lasers. Applied Optics 16, 46–56.

Kirk, J.T., 1994. Light and Photosynthesis in Aquatic Ecosystems, second ed., vol. XVI. Cambridge Univ. Press, Cambridge, 509 pp.

Kokalj, Ž., Zakšek, K., Oštir, K., 2011. Application of sky-view factor for the visualisation of historic landscape features in lidar-derived relief models. Antiquity 85, 263–273.

Kunz, G.J., Lamberts, C.W., van Mierlo, G.W.M., Vries, F.P.P. de, Visse, H., Smorenburg, C., Spitzer, D., Hofstraat, H., Dirks, R.W.J., 1992. Laser bathymetry in the Netherlands. In: EARSeL Advances in Remote Sensing, pp. 36–41.

Lambeck, K., Anzidei, M., Antonioli, F., Benini, A., Esposito, A., 2004. Sea level in Roman time in the Central Mediterranean and implications for recent change. Earth and Planetary Science Letters 224, 563–575.

Lambrick, G., 2008. Air and Earth: Aerial Archaeology in Ireland: a Review for the Heritage Council. Heritage Council, Kilkenny.

Lee, Z.P., Du, K., Voss, K.J., Zibordi, G., Lubac, B., Arnone, R., Weidemann, A., 2011. An inherent-optical-property-centered approach to correct the angular effects in water-leaving radiance. Applied Optics 50, 3155–3167.

Long, B.F., Aucoin, F., Montreuil, S., Robitaille, V., Xhardé, R., 2010. Airborne LiDAR bathymetry applied to coastal hydrodynamic processes. In: Proceedings of the International Conference on Coastal Engineering. 32.

Mandlburger, G., Otepka, J., Karel, W., Wagner, W., Pfeifer, N., 2009. Orientation and processing of airborne laser scanning data (OPALS) - concept and first results of a comprehensive ALS software. In: International Archives of the Photogrammetry, Remote Sensing and Spatial Information Sciences, vol. 38 (Part 3/W8), pp. 55–60. Paris, France.

Mandlburger, G., Pfennigbauer, M., Steinbacher, F., Pfeifer, N., 2011. Airborne Hydrographic LiDAR Mapping – potential of a new technique for capturing shallow water bodies. In: Chan, F., Marinova, D., Anderssen, R. (Eds.), MODSIM2011, 19th International Congress on Modelling and Simulation. Modelling and Simulation Society of Australia and New Zealand, December 2011, Perth, pp. 2416–2422.

Marcus, W.A., Fonstad, M.A., 2008. Optical remote mapping of rivers at sub-meter resolutions and watershed extents. Earth Surface Processes and Landforms 33 (1), 4–24.

McNair, G., 2010. Coastal Zone Mapping with Airborne LiDAR Bathymetry. Master thesis, Ås.

Mobley, C.D., 1994. Light and Water: Radiative Transfer in Natural Waters, vol. XVII. Academic Press, San Diego, 592 pp.

Mobley, C.D., Stramski, D., Bissett, W.P., Boss, E., 2004. Optical modeling of ocean water. Is the case 1–case 2 classification still useful? Oceanography 17, 60–67.

Mullen, L., 2009. Optical propagation in the underwater environment. In: Proceedings of Atmospheric Propagation VI, Orlando, Florida, United States. 30 April 2009. SPIE, Bellingham, pp. 732409–732409-9.

Piech, K.R., Walker, J.E., 1971. Aerial color analysis of water quality. Journal of the Surveying and Mapping Division. Proceedings of the American Society of Civil Engineers 97, 185–197.
Pfennigbauer, M., Ullrich, A., 2009. The new RIEGL V-Line laser scanner's higher data quality using new measurement principles. In: Optical 3D Measurement Techniques, Vienna.
Prahov, N., Angelova, H., Kotsev, A., Popov, A., Dimitrov, S., 2011. Predictive modeling in archaeology: world practice and Bulgarian perspectives. Bulgarian e-Journal of Archaeology 1, 71–121.
Ressl, C., Mandlburger, G., Pfeifer, N., 2009. Investigating adjustment of airborne laser scanning strips without usage of GNSS/IMU trajectory data. In: ISPRS Workshop Laserscanning '09, IAPRS, vol. XXXVIII, Part 3/W8, pp. 195–200.
Riegl, 2012. VQ-820-G Data Sheet. URL: http://www.riegl.com/nc/products/airborne-scanning/produktdetail/product/scanner/32/ (last accessed 31.10.12.).
Silva, T.S.F., Costa, M.P.F., Melack, J.M., Novo, E.M.L.M., 2008. Remote sensing of aquatic vegetation: theory and applications. Environmental Monitoring and Assessment 140, 131–145.
Smith, R.C., Baker, K.S., 1981. Optical properties of the clearest natural waters (200–800 nm). Applied Optics 20, 177–184.
Strachan, D., 1995. Problems and potentials of coastal reconnaissance in Essex. AARGNews 10, 28–35.
Wang, C.-K., Philpot, W.D., 2007. Using airborne bathymetric lidar to detect bottom type variation in shallow waters. Remote Sensing of Environment 106, 123–135.
Wehr, A., Lohr, U., 1999. Airborne laser scanning – an introduction and overview. ISPRS Journal of Photogrammetry and Remote Sensing 54 (2–3), 68–82.
Westaway, R.M., Lane, S.N., Hicks, D.M., 2001. Remote sensing of clear water, shallow, gravel-bed rivers using digital photogrammetry. Photogrammetric Engineering & Remote Sensing 67 (11), 1271–1281.
Westley, K., Quinn, R., Forsythe, W., Plets, R., Bell, T., Benetti, S., McGrath, F., Robinson, R., 2010. Mapping Submerged Landscapes Using Multibeam Bathymetric Data: a case study from the north coast of Ireland. The International Journal of Nautical Archaeology 40 (1), 99–112.
Wojtanowski, J., Mierczyk, Z., Zygmunt, M., 2008. Laser remote sensing of underwater objects. In: Remote Sensing of the Ocean, Sea Ice, and Large Water Regions 2008, Cardiff, Wales, United Kingdom. 15 September 2008. SPIE, Bellingham, p. 71050F.
Wozencraft, J., Millar, D., 2005. Airborne lidar and integrated technologies for coastal mapping and Nautical charting. Marine Technology Society Journal 39 (3), 27–35.
Yokoyama, R., Sirasawa, M., Pike, R.J., 2002. Visualizing topography by openness: a new application of image processing to digital elevation models. Photogrammetric Engineering & Remote Sensing 68 (3), 257–265.